

Streaming-dLLM: Accelerating Diffusion LLMs via Suffix Pruning and Dynamic Decoding

Zhongyu Xiao¹ Zhiwei Hao² Jianyuan Guo² Yong Luo³ Jia Liu⁴ Jie Xu⁵ Han Hu¹

Abstract

Diffusion Large Language Models (dLLMs) offer a compelling paradigm for natural language generation, leveraging parallel decoding and bidirectional attention to achieve superior global coherence compared to autoregressive models. While recent works have accelerated inference via KV cache reuse or heuristic decoding, they overlook the intrinsic inefficiencies within the block-wise diffusion process. Specifically, they suffer from spatial redundancy by modeling informative-sparse suffix regions uniformly and temporal inefficiency by applying fixed denoising schedules across all the decoding process. To address this, we propose Streaming-dLLM, a training-free framework that streamlines inference across both spatial and temporal dimensions. Spatially, we introduce attenuation guided suffix modeling to approximate the full context by pruning redundant mask tokens. Temporally, we employ a dynamic confidence aware strategy with an early exit mechanism, allowing the model to skip unnecessary iterations for converged tokens. Extensive experiments show that Streaming-dLLM achieves up to $68.2\times$ speedup while maintaining generation quality, highlighting its effectiveness in diffusion decoding. The code is available at <https://github.com/xiaoshideta/Streaming-dLLM>.

1. Introduction

Diffusion Large Language Models (dLLMs) have gained emerged as a promising generative paradigm in natural lan-

¹School of information and Electronics, Beijing Institute of Technology, Beijing ²Department of Computer Science, City University of Hong Kong, Hong Kong ³School of Computer Science, Wuhan University, Wuhan ⁴School of Economics and Management, Communication University of China, Beijing ⁵School of Science and Engineering, The Chinese University of Hong Kong (Shenzhen), Shenzhen. Correspondence to: Han Hu <hhu@bit.edu.cn>.

Preprint. January 28, 2026.

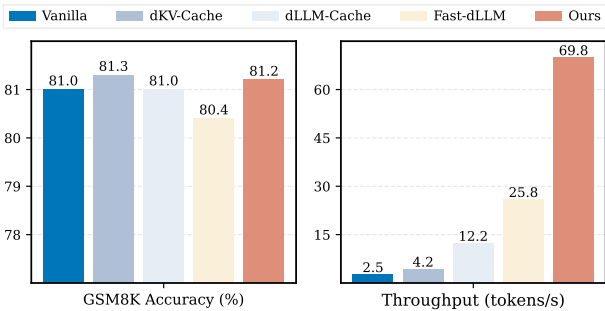


Figure 1. Comparison of accuracy and throughput across different acceleration strategies. Our proposed method improves inference throughput while maintaining competitive accuracy compared to prior approaches.

guage processing (Nie et al., 2025; Ye et al., 2025; Zhu et al., 2025a;b; You et al., 2025; Sahoo et al., 2024). In contrast to traditional autoregressive Large Language models (LLMs) (Achiam et al., 2023; Guo et al., 2025; Dubey et al., 2024; Yang et al., 2025), dLLMs employ parallel decoding with bidirectional attention, enabling simultaneous information integration across all sequence positions and fostering superior global coherence and semantic consistency (Li et al., 2022; Arriola et al., 2025). This architectural shift is expected to alleviate the sequential inference bottleneck and the unidirectional context dependency inherent in autoregressive generation.

Despite these advantages, existing dLLMs lag significantly behind autoregressive models in inference speed (Li et al., 2025; Zhang et al., 2025). This gap primarily arises from the intrinsic nature of diffusion decoding. In particular, token representations evolve continuously across denoising steps, which prevents the effective reuse of the highly optimized Key-Value (KV) Cache. Furthermore, parallel generation amplifies sensitivity to decoding uncertainty, often necessitating additional denoising iterations to preserve generation quality.

Consequently, improving the inference efficiency of dLLMs has attracted substantial attention recently (Wu et al., 2023; 2025a; Liu et al., 2025a; Zhao et al., 2025; Liu et al., 2025b; Wei et al., 2025; Chen et al., 2025a; Tian et al., 2025; Ma et al., 2025b). For instance, dKV-Cache (Ma et al., 2025a)

exploits the partial stability of token states to enable limited cache reuse, while Fast-dLLM (Wu et al., 2025b) adopts semi-autoregressive block-wise generation combined with confidence decoding. While these approaches achieve noticeable acceleration, they overlook the fundamental redundancy deeply rooted in the block-wise diffusion process. **Spatially**, mask tokens in the suffix region carry limited and homogeneous information, yet standard attention mechanisms process every suffix token at every step. Since the suffix region scales with the target generation length, the model wastes substantial computation on low value mask positions during the early and middle stages of diffusion. **Temporally**, the uncertainty within each generation block converges at varying rates. However, conventional thresholding strategies apply a static criterion, failing to adapt to this dynamic behavior. Consequently, high confidence tokens are often forced back into a masked state in subsequent iterations, which restricts the effective throughput of parallel decoding and may disrupt the refinement of truly uncertain tokens.

To address these challenges, we propose **Streaming-dLLM**, a training-free framework for fast and scalable inference. Our method is motivated by two key observations: the diminishing attention influence of distant suffix tokens and the dynamic evolution of token confidence within generation blocks. To tackle spatial inefficiency, we introduce attenuation-guided suffix modeling. Instead of attending to the entire suffix, we preserve only a small set of informative suffix blocks alongside positional cues of the final length to approximate the global context. This design drastically reduces the computational cost of iterative inference without compromising generation quality. To address temporal inefficiency, we propose a dynamic confidence aware parallel decoding strategy. This mechanism adaptively adjusts decoding thresholds based on both the diffusion stage and the intra-block confidence distribution. Furthermore, we incorporate an early exit mechanism to terminate decoding immediately upon predicting the End-of-Sequence (EOS) token, avoiding unnecessary computation for the remainder of the block sequence. Streaming-dLLM integrates these complementary components to optimize decoding along both spatial and temporal dimensions. Extensive experiments demonstrate that our approach achieves up to $68.2\times$ inference speedup without degrading downstream performance.

Our contributions are summarized as follows:

- We propose attenuation guided suffix modeling, a training-free approach that accelerates inference by pruning redundant suffix attention during the decoding process.
- We develop a dynamic confidence aware parallel decod-

ing strategy that flexibly adjusts parallelism according to real-time decoding uncertainty, enabling plug-and-play inference acceleration.

- Extensive experiments across multiple dLLMs and benchmarks demonstrate that Streaming-dLLM significantly improves inference throughput with negligible impact on generation quality.

2. Related works

2.1. Diffusion Language Models

Diffusion models have emerged as a highly promising generative paradigm for text, serving as an alternative to autoregressive models based on a forward masking and reverse denoising process (Li et al., 2025; Zhu et al., 2025c). In general, existing dLLMs are broadly categorized into continuous space (Li et al., 2022; Yu et al., 2022; Lin et al., 2023; Gao et al., 2024; Mahabadi et al., 2024) and discrete space (Austin et al., 2021a; Nie et al., 2025; Song et al., 2025b; Ye et al., 2025; Zhu et al., 2025a) approaches, depending on the space in which diffusion is performed.

Focusing on continuous space, Diffusion-LM (Li et al., 2022) pioneers this direction by applying Gaussian diffusion directly to token embeddings. GENIE (Lin et al., 2023) introduces a large scale pretraining strategy with a paragraph level denoising objective that reconstructs corrupted text spans, enabling effective learning from massive corpora. In contrast, discrete space dLLMs define diffusion directly over the token vocabulary. D3PM (Austin et al., 2021a) defines the forward noising procedure as a discrete Markov chain with a predefined transition matrix. LLaDA (Nie et al., 2025) further advances this line of work by training discrete diffusion language models from scratch using a masked-token cross entropy objective. Overall, dLLMs have demonstrated strong empirical performance across multiple benchmarks and are becoming increasingly competitive with leading autoregressive language models.

2.2. Acceleration Techniques for dLLMs

To fully unleash the potential of dLLMs, recent studies have explored various inference (Feng et al., 2025). In terms of caching mechanisms, dKV-Cache (Ma et al., 2025a) introduces a delayed KV Cache to reduce redundant memory usage, while Elastic-Cache (Nguyen-Tri et al., 2025) leverages attention aware drift to perform adaptive KV refreshes, thereby improving cache efficiency. Regarding parallel decoding, Fast-dLLM (Wu et al., 2025b) proposes a confidence threshold parallel decoding to accelerate the diffusion process. ReMDM (Wang et al., 2025) introduces a remasking sampler at inference, allowing the model to revise previously generated tokens and achieve a flexible trade-off between computational cost and generation quality.

For model pruning, DPad (Chen et al., 2025b) prunes redundant regions by sampling suffix windows, and Sparse-dLLM (Song et al., 2025a) dynamically removes low importance KV entries from both prefix and suffix tokens to reduce inference overhead. Nevertheless, these methods remain constrained by the intrinsic characteristics of the block-wise diffusion decoding, often exhibiting spatial redundancy and temporal inefficiency during generation, which limits their potential for further acceleration.

3. Method

3.1. Preliminary

Contrary to autoregressive LLMs, dLLMs perform inference through iterative decoding, where masked tokens are progressively reconstructed into the final output over discrete diffusion steps T . For a generation task with target length L , the initial sequence is defined as:

$$x^{(0)} = [p_0, \underbrace{[\text{MASK}], \dots, [\text{MASK}]}_L], \quad (1)$$

where $x^{(t)}$ denotes the state of the entire sequence at time $t \in [0, T]$, p_0 represents the input prompt and $[\text{MASK}]$ indicates a masked token. The masked sequence of length L is partitioned into N non-overlapping blocks with K tokens in each block, such that $L = N \times K$. For block $B_n^{(t)}$, $n \in \{0, \dots, N-1\}$:

$$\begin{aligned} I_n &= \{p_L + nK, \dots, p_L + (n+1)K - 1\}, \\ B_n^{(t)} &= x_{I_n}^{(t)} = \left[x_{p_L+nK}^{(t)}, \dots, x_{p_L+(n+1)K-1}^{(t)} \right]. \end{aligned} \quad (2)$$

Here, I_n denotes the token indices in the n -th block, and p_L is the index offset corresponding to the prompt length. This generation paradigm is referred to as block-wise diffusion decoding. In particular, when $K = 1$, the decoding process degenerates into an autoregressive-like generation scheme. Contrastively, when $K = L$, it simplifies to pure diffusion decoding with all tokens generated in parallel.

Each block is decoded over M diffusion steps ($T = N \times M$). At iteration $t \in \{0, \dots, M-1\}$, the model predicts logits for all positions:

$$z^{(t)} = f_\theta(x^{(t)}), \quad (3)$$

where f_θ denotes the dLLMs parameterized by θ . Sampling and token prediction are then performed only for positions $i \in B_n$ where $x_i^{(t)} = [\text{MASK}]$:

$$\begin{aligned} c_i^{(t)} &= \max(\text{Softmax}(z_i^{(t)})), \\ \hat{x}_i^{(t)} &= \arg \max(\text{Softmax}(z_i^{(t)})). \end{aligned} \quad (4)$$

Finally, token states are updated according to:

$$x_i^{(t+1)} = \begin{cases} \hat{x}_i^{(t)}, & i \in \{i_k \mid S(\hat{x}_{i_k}^{(t)}, c_{i_k}^{(t)})\}, \\ x_i^{(t)}, & \text{otherwise.} \end{cases} \quad (5)$$

where $S(\cdot)$ denotes the token selection strategy, which determines the subset of positions to be updated based on predicted tokens and their corresponding confidence scores. The decoding iteration for block n terminates when $\{i \in B_n \mid x_i = [\text{MASK}]\} = \emptyset$, after which the model proceeds to decode block $n+1$.

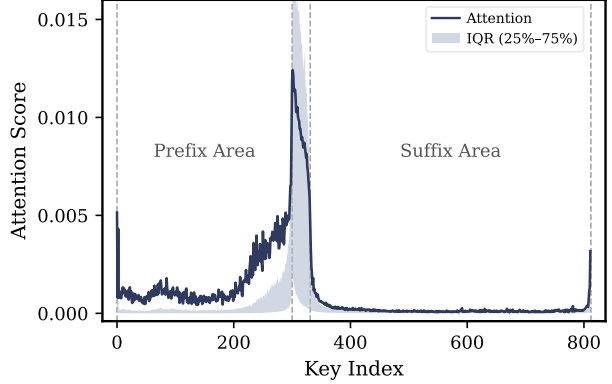


Figure 2. Attention distribution at the final layer (Layer 31) of LLaDA-1.5, showing interactions between the current block and the full input sequence. The solid line denotes the mean attention score at each diffusion step, the shaded region represents the interquartile range (IQR, 25%–75%), and gray dashed lines delineate the prefix, current-generation and suffix regions. Attention is concentrated on a few neighboring suffix blocks and the final token and most intermediate suffix positions receive negligible attention, highlighting redundancy in the suffix during block generation.

3.2. Rethinking Inference of dLLMs

Diffusion language models leverage bidirectional attention and parallel decoding to exploit global contextual information, thereby improving generation quality. However, whether this design remains necessary and efficient at every diffusion step during inference, especially for long text generation, has yet to be systematically examined.

In the diffusion decoding framework (Equation 3), bidirectional attention is computed over the full sequence $x^{(t)}$ at each prediction. Unlike autoregressive models, the input sequence of dLLMs consists of a semantically dense prompt region and a large number of ungenerated mask tokens. When the prompt is short and the generation length is large, the model is forced to repeatedly attend to an extensive masked region, which incurs substantial computational overhead. As masked tokens, these positions also provide a large amount of homogeneous semantic information, while whether such information is actually necessary or effective during generation remains unclear.

To investigate this, we analyze attention distribution between the currently generated block and the entire input sequence. As shown in Figure 2, attention over the suffix region decays with distance. Although the suffix consti-

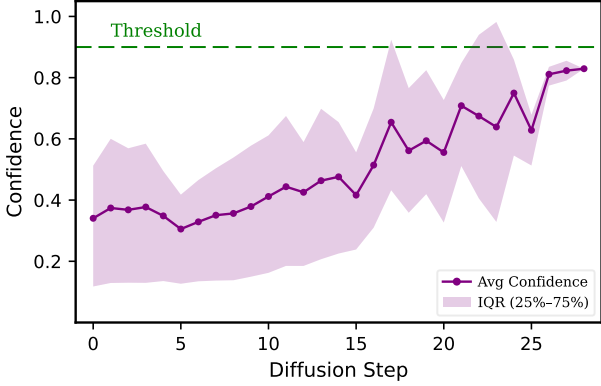


Figure 3. Token confidence distribution during iterative block-wise generation of LLaDA-1.5 on GSM8K with a generation length of 256, showing that mean token confidence steadily increases over iterations. The solid line denotes the mean confidence at each diffusion step and the shaded area represents the interquartile range (IQR, 25%–75%). While a high confidence threshold ensures generation quality, it can be conservative, potentially delaying the acceptance of sufficiently confident tokens. Visualizations of additional blocks are provided in the Section A.

tutes most of the sequence, many intermediate positions receive near-zero scores. Conversely, the current generation block primarily attends to a small number of neighboring blocks within the suffix region, as well as the token at the end position. This suggests that only a limited portion of the suffix mask region contains meaningful structural information, while the remaining positions largely serve as redundant placeholders. Further details and discussions regarding the Figure 2 are provided in the Section A.

Meanwhile, we further examine the evolution behavior of token confidence during the parallel decoding process within the block. Previous method (Wu et al., 2025b) typically uses a fixed confidence threshold to determine whether a token should be updated, which implicitly assumes that the confidence distribution remains relatively stable during decoding. In light of this, we collect statistics from the iterative decoding process on 100 GSM8K samples and visualize the first generated block. As shown in Figure 3, the number of remaining masked tokens within the current block steadily decreases as diffusion progresses, while the confidence distribution undergoes substantial contraction and shift. Moreover, we plot token confidences within the interquartile range (IQR, 25% – 75%), which better reflects the typical behavior of most tokens during decoding. The observation indicate that using a fixed confidence threshold is suboptimal: early steps require a high threshold to ensure generation quality, while later steps benefit from a lower threshold to allow timely token acceptance and improve parallel decoding efficiency.

Overall, above analysis reveals two complementary inefficiencies in the reasoning process of dLLMs: (1) Spatially, a substantial amount of computation is devoted to suffix mask tokens that carry limited semantic information, leading to a clear mismatch between computation and informative content. (2) Temporally, the fixed confidence decoding strategy fails to capture the dynamic evolution of uncertainty within a block, forcing tokens with sufficient confidence to participate in needless diffusion steps. These observations motivate our redesign of both the suffix modeling approach and the decoding strategy for the reasoning stage.

3.3. Streaming-dLLM

Motivated by the two inefficiencies identified above, we propose Streaming-dLLM, a training-free framework designed to accelerate dLLMs inference. The core insight is to streamline block-wise diffusion decoding by progressively eliminating redundant computation along both spatial and temporal dimensions. In response to spatial redundancy in the suffix region, when decoding the n -th block, Streaming-dLLM first applies attenuation guided suffix modeling to retain only a minimal set of structural cues that are most critical for generating the current block. In parallel, to reflect the dynamic confidence evolution, we further adapts the parallel decoding strategy during intra-block diffusion iterations according to the evolving token confidence distribution, allowing high confidence tokens to be finalized earlier. Additionally, we incorporate an early exit mechanism to terminate decoding once the EOS token is predicted.

Attenuation Guided Suffix Modeling. Following Equations 1 and 2, the sequence at diffusion step t is:

$$x^{(t)} = [p_0, \hat{B}_0^{(t)}, \dots, \hat{B}_{c-1}^{(t)}, B_c^{(t)}, \dots, B_{N-1}^{(t)}], \quad (6)$$

where $\hat{B}_i^{(t)}, i \in [0, c-1]$ denotes the blocks that have already been decoded. Together with the input prompt p_0 , they form the prefix region $S_{\text{prefix}}^{(t)}$. $B_c^{(t)}$ represents the block being decoded at diffusion step t , referred to as the current region $S_{\text{current}}^{(t)}$. The remaining blocks $B_j^{(t)}$ for $j \in (c, N-1]$ constitute the suffix region $S_{\text{suffix}}^{(t)}$.

For the suffix region, we adopt a sliding window strategy that retains only w blocks closest to $S_{\text{current}}^{(t)}$. In addition, we preserve the positional information of the final token to provide a coarse representation of the entire suffix while maintaining the logical ordering of tokens via RoPE (Su et al., 2024) position IDs.:

$$\begin{aligned} \tilde{I} &= \{I_c, \dots, I_{c+w}\} \cup \{p_L + L\}, \\ \tilde{S}_{\text{suffix}}^{(t)} &= \bigcup_{I_S \in \tilde{I}} S_{\text{suffix}}^{(t)}. \end{aligned} \quad (7)$$

The approximated suffix is then concatenated with the prefix and current regions to form the input sequence at diffusion

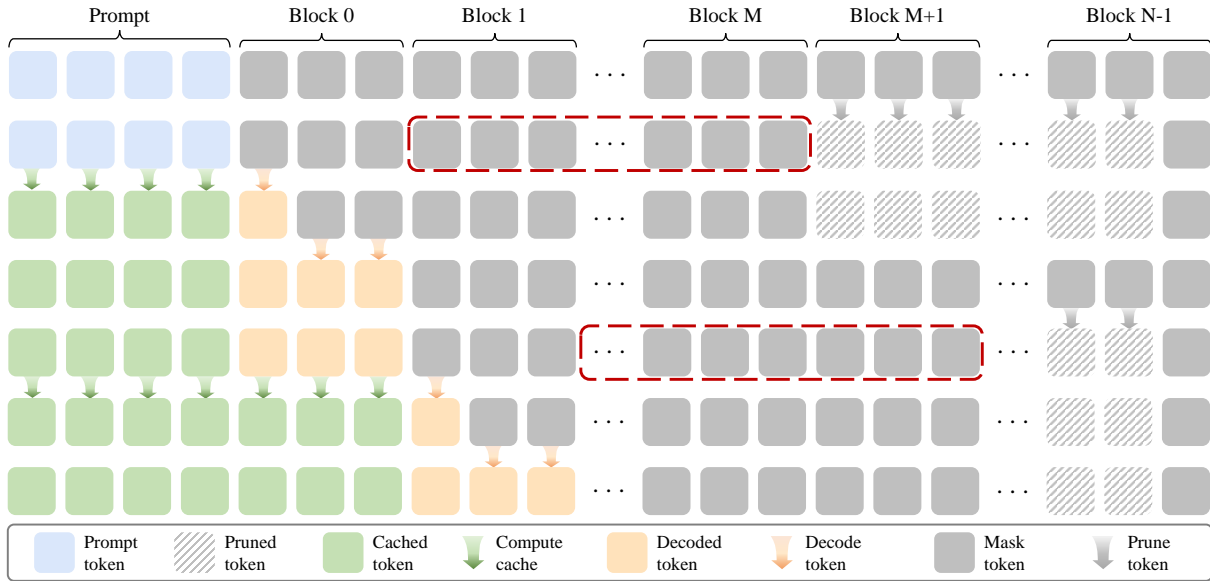


Figure 4. Illustration of Attenuation-Guided Suffix Modeling. For each block, the nearest neighboring region following the current block is retained using a sliding window (red dashed box) and concatenated with the trailing position to form an approximate suffix region.

step t , which is subsequently fed into the diffusion language model for prediction.

$$\tilde{x}^{(t)} = S_{\text{prefix}}^{(t)} \cup S_{\text{current}}^{(t)} \cup \tilde{S}_{\text{suffix}}^{(t)}, \quad (8)$$

This approximation is guided by the observation from Figure 2. During the generation of $S_{\text{current}}^{(t)}$, the suffix region primarily provides coarse structural constraints, such as positional continuity and termination cues, rather than detailed semantic information. Meanwhile, tokens in the distant suffix remain highly uncertain throughout most diffusion steps, limiting their contribution to refining the current block.

Accordingly, we retain only the suffix blocks adjacent to $S_{\text{current}}^{(t)}$ along with the terminal positional token, which preserves the essential structural signals required for stable decoding. This design significantly reduces redundant computation in both attention and denoising, while maintaining global coherence across blocks.

Dynamic Confidence Aware Parallel Decoding. During iterative block-wise decoding, the KV representations of the prefix region are computed once at the first diffusion step and reused across all subsequent steps within the same block. This approach significantly reduces redundant attention computation on the prefix while preserving information from previously decoded tokens (Wu et al., 2025b).

In the prediction forward, the query vectors are constructed from the current generation region $S_{\text{current}}^{(t)}$ together with the approximated suffix region $\tilde{S}_{\text{suffix}}^{(t)}$. These queries attend to the KV representations of the entire sequence $\tilde{x}^{(t)}$ to perform attention computation. Attention scores are sub-

sequently processed by the remaining model components to produce the prediction logits. Following Equation 4, we obtain generated token $\hat{x}_i^{(t)}$ for each position within query area, along with its corresponding confidence score $c_i^{(t)}$. The confidence scores are used to determine whether a token can be finalized at the current diffusion step. We define a confidence-aware selection function $S(\cdot)$ that decides whether a predicted token $\hat{x}_{i_k}^{(t)}$ is accepted according to its confidence $c_{i_k}^{(t)}$. Tokens whose confidence exceeds the threshold $\tau^{(t)}$ are finalized, while the remaining tokens stay masked and continue to be refined in subsequent diffusion iterations. When no token satisfies the confidence threshold, we finalize the masked token with the highest confidence. Formally, the selection rule can be defined as:

$$S(\hat{x}_i^{(t)}, c_i^{(t)}) = \begin{cases} \hat{x}_i^{(t)}, & c_i^{(t)} \geq \tau^{(t)}, \\ \hat{x}_{\arg \max_i c_i^{(t)}}^{(t)}, & \forall i, c_i^{(t)} < \tau^{(t)}, \\ \text{None}, & \text{otherwise.} \end{cases} \quad (9)$$

To account for the evolving uncertainty during block-wise diffusion, we adopt an adaptive threshold that varies with the proportion of masked tokens in the current query. The threshold at step t is defined as:

$$\tau^{(t)} = \tau_0 (1 - \alpha(1 - r_{\text{mask}})), \quad (10)$$

where τ_0 denotes the base confidence threshold, α controls the adaptation strength, and r_{mask} represents the ratio of masked tokens at the current decoding step. By this adaptive design, we can further exploit the parallel decoding potential of diffusion language models, achieving a flexible trade-off between inference speed and accuracy.

Table 1. Comparison of Dream-Base suite performance across four benchmarks at different generation lengths (256 and 512). Each cell reports accuracy (top) and decoding throughput with relative speedup over the Dream baseline (bottom; blue: tokens/s, orange: speedup). Results in bold indicate the highest score, while those underlined denote the second-best performance for each method. ‘*’ marks results we reproduced using the official implementation, as they were not reported in the original papers.

Benchmark	Gen Length	Dream	dKV-Cache	Prefix-Cache	Fast-dLLM	Ours
HumanEval (0-shot)	256	49.4	48.2*	<u>53.7</u>	54.3	54.3
	512	20.4 (1×)	21.5 (1.1×)	<u>32.0 (1.6×)</u>	<u>53.7 (2.6×)</u>	<u>74.7 (3.7×)</u>
		54.3	49.4*	54.9	54.3	<u>54.6</u>
GSM8K-CoT (5-shot)	256	74.8	73.6*	<u>74.0</u>	73.5	<u>74.0</u>
	512	<u>9.0 (1×)</u>	<u>17.0 (1.9×)</u>	<u>31.5 (3.5×)</u>	<u>47.9 (5.3×)</u>	<u>75.5 (8.4×)</u>
		<u>74.2</u>	71.6*	<u>74.2</u>	74.1	74.7
MBPP (3-shot)	256	56.6	54.0*	53.2	<u>56.4</u>	<u>56.4</u>
	512	<u>11.0 (1×)</u>	<u>14.7 (1.3×)</u>	<u>32.3 (2.9×)</u>	<u>67.2 (6.1×)</u>	<u>80.2 (7.3×)</u>
		55.6	53.0*	53.8	55.2	55.8
MATH (4-shot)	256	38.4	36.8*	36.8	<u>37.6</u>	<u>37.6</u>
	512	<u>10.5 (1×)</u>	<u>14.6 (1.4×)</u>	<u>32.5 (3.1×)</u>	<u>62.6 (5.98×)</u>	<u>78.4 (7.5×)</u>
		39.8	38.5*	38.0	39.3	<u>39.4</u>
		<u>8.6 (1×)</u>	<u>11.6 (1.3×)</u>	<u>24.5 (2.8×)</u>	<u>54.4 (6.3×)</u>	<u>96.0 (11.2×)</u>

Early Exit For Block Diffusion. To further improve inference efficiency, we introduce an early exit mechanism for block-wise diffusion decoding. During generation, if a block predicts the EOS token with high confidence, all subsequent blocks are skipped. This strategy prevents unnecessary computation on remaining blocks, reducing inference latency while ensuring that the generated sequence remains complete. By leveraging this property, Streaming-dLLM can adaptively reduce the decoding steps without compromising sequence integrity, further enhancing efficiency in text generation scenarios.

4. Experiment

4.1. Experimental Setup

To evaluate the effectiveness of Streaming-dLLM, we conduct experiments on representative dLLMs including Dream-v0-7B-Base (Ye et al., 2025), LLaDA-8B-Instruct (Nie et al., 2025), and LLaDA-1.5 (Zhu et al., 2025a). The proposed method is compared with the corresponding vanilla implementations as well as recent state-of-the-art dLLM inference acceleration methods (Ma et al., 2025a; Wu et al., 2025b). We report results across a diverse set of domains, covering mathematical and scientific reasoning tasks (GSM8K (Cobbe et al., 2021), MATH (Hendrycks et al., 2020)) as well as code generation benchmarks (HumanEval (Chen, 2021), MBPP (Austin et al., 2021b)). In addition, we assess the models under varying generation

lengths to examine the scalability and robustness of the proposed approach.

Our metrics capture both generation quality and inference efficiency, measured by benchmark accuracy, throughput (tokens per second, TPS) and inference latency per sample. For throughput computation, we count only non EOS tokens across the entire generated sequence, which ensures the reliability and comparability of the reported results. All experiments are conducted within the lm-eval framework to ensure consistency and reproducibility, using a single NVIDIA A800 80GB GPU. Additional optimization details are provided in the Section B.3.

4.2. Main Result

As shown in Table 1, Our method achieves 3.7×–13.3× speedup across all benchmarks over the vanilla backbone. Compared with the state-of-the-art acceleration method, it provides 1.5×–2.3× additional speedup on tasks with a generation length of 512. Meanwhile, our accuracy was comparable or slightly better, which demonstrates the effectiveness of our approach.

In addition, more experiments on LLaDA-1.5 show even greater throughput improvements, as presented in Table 2. In particular, Streaming-dLLM achieves a speedup of 68.2× on MBPP tasks with a generation length of 512, which substantially exceeds that of Fast-dLLM (Wu et al., 2025b). Similar performance improvements are observed on the

Table 2. Comparison of LLaDA-1.5 suite performance across four benchmarks at different generation lengths (256 and 512). Each cell reports accuracy (top) and decoding throughput with relative speedup over the LLaDA-1.5 baseline (bottom; blue: tokens/s, orange: speedup). Results in bold indicate the highest score, while those underlined denote the second-best performance for each method. ^{*,} marks results we reproduced using the official implementation, as they were not reported in the original papers.

Benchmark	Gen Length	LLaDA-1.5	dKV-Cache	Prefix-Cache	Fast-dLLM	Ours
HumanEval (0-shot)	256	43.9*	<u>40.2*</u>	38.4*	37.2*	39.0
	512	<u>6.4 (1×)</u>	6.6 (1.0×)	<u>10.9 (1.7×)</u>	19.1 (3.0×)	<u>34.1 (5.3×)</u>
		40.5*	<u>40.2*</u>	37.8*	39.8*	<u>40.2</u>
		<u>2.9 (1×)</u>	<u>3.3 (1.1×)</u>	<u>4.8 (1.7×)</u>	<u>13.6 (4.7×)</u>	<u>26.7 (9.2×)</u>
GSM8K (5-shot)	256	80.5*	80.7*	80.6*	80.7	80.8
	512	<u>6.3 (1×)</u>	10.8 (1.7×)	<u>24.4 (3.9×)</u>	<u>50.0 (7.9×)</u>	<u>66.2 (10.5×)</u>
		81.0*	81.3*	81.0*	80.4	<u>81.2</u>
		<u>2.5 (1×)</u>	<u>4.2 (1.7×)</u>	<u>8.2 (3.3×)</u>	<u>25.8 (10.3×)</u>	<u>69.8 (28.0×)</u>
MBPP (3-shot)	256	<u>38.0*</u>	38.2*	37.8*	37.6*	37.8
	512	<u>2.2 (1×)</u>	<u>3.5 (1.6×)</u>	<u>7.6 (3.5×)</u>	<u>29.5 (13.4×)</u>	<u>54.7 (24.9×)</u>
		38.2*	38.1*	38.0*	38.1*	38.4
		<u>0.9 (1×)</u>	<u>1.5 (1.7×)</u>	<u>2.8 (3.1×)</u>	<u>16.5 (18.3×)</u>	<u>61.4 (68.2×)</u>
MATH (4-shot)	256	<u>32.7*</u>	31.8*	32.5*	32.6	33.7
	512	<u>7.8 (1×)</u>	12.4 (1.6×)	<u>25.9 (3.3×)</u>	<u>47.1 (6.0×)</u>	<u>66.2 (8.5×)</u>
		37.1*	<u>35.1*</u>	35.0*	<u>35.1</u>	<u>35.1</u>
		<u>4.8 (1×)</u>	<u>7.5 (1.6×)</u>	<u>13.9 (2.9×)</u>	<u>38.3 (7.9×)</u>	<u>62.4 (13.0×)</u>

LLaDA-Instruct and more results are provided in Section B.1.

Additional results on inference latency are provided in the Section B.2. Compared with Fast-dLLM, Streaming-dLLM achieves up to 85.5% reduction in inference latency per sample, indicating that our method not only improves throughput but also shortens real world response time. Overall, these results highlight the effectiveness and generalizability of our method across multiple model and benchmarks.

4.3. Ablation Result

In order to comprehensively evaluate our approach, we conduct ablation study on the GSM8K dataset using LLaDA-1.5 as the default model.

Ablation of each module. To evaluate the effectiveness of the key components in our approach, we conduct ablation studies on three core modules: Attenuation Guided Suffix Modeling, Dynamic Confidence Aware Parallel Decoding and Early Exit for Block Diffusion. The results are summarized in Table 3. When all three modules are enabled, the model achieves the largest throughput improvement, and this trend remains consistent across different dLLMs. This improvement is partly attributable to attenuation guided suffix modeling, which reduces computational complexity and may also enhance generation quality by mitigating interference from redundant suffix regions, as evidenced by a slight yet consistent gain. Such findings highlight its potential

Table 3. Ablation study on the components of our proposed method. The results are on the GSM8K dataset (Dream uses the GSM8K-CoT version) using LLaDA-1.5 for a generation length of 512. Each component contributes to the overall performance. **Suf.:** Attenuation Guided Suffix Modeling, **Dyn.:** Dynamic Confidence Aware Parallel Decoding, **Exit.:** Early Exit for Block Diffusion.

Model	Suf.	Dyn.	Exit.	Acc. (%)	Th.(tok/s)
Dream	✗	✗	✗	74.1	41.7
	✓	✗	✗	74.6	76.8
	✓	✓	✗	74.7	82.2
	✓	✓	✓	74.7	94.1
LLaDA	✗	✗	✗	77.2	32.1
	✓	✗	✗	78.6	46.9
	✓	✓	✗	78.7	52.4
	✓	✓	✓	78.7	65.9
LLaDA-1.5	✗	✗	✗	80.4	25.8
	✓	✗	✗	81.4	44.9
	✓	✓	✗	81.2	50.3
	✓	✓	✓	81.2	69.8

as a direction for future study in general dLLMs. Then, when dynamic confidence aware parallel decoding is activated, the generation quality exhibits moderate fluctuations. We attribute this behavior to the asynchronous evolution of token level confidence under parallel decoding, which introduces mild uncertainty perturbations at certain diffusion iterations. Finally, introducing early exit does not degrade generation quality, suggesting that the original diffusion language model is inherently robust during inference and

Table 4. Impact of few-shots on Accuracy and Speedup for LLaDA-1.5 on GSM8K (5-Shot).

Model	3-shot	5-shot	8-shot
LLaDA-1.5	80.1 3.4 (1 \times)	81.0 2.5 (1 \times)	81.7 1.7 (1 \times)
Fast-dLLM	79.7 36.5 (10.7 \times)	80.4 25.8 (10.3 \times)	79.9 20.9 (12.3 \times)
Ours	80.2 77.4 (22.8 \times)	81.2 69.8 (28.0 \times)	81.5 61.3 (36.1 \times)

Table 5. Impact of generation length on Accuracy and Speedup for LLaDA-1.5 on GSM8K (5-Shot).

Model	512	1024	2048
LLaDA-1.5	81.0 2.5 (1 \times)	81.2 0.8 (1 \times)	81.2 0.3 (1 \times)
Fast-dLLM	80.4 25.8 (10.3 \times)	80.5 12.3 (15.4 \times)	80.7 5.1 (17.0 \times)
Ours	81.2 69.8 (28.0 \times)	81.2 64.9 (81.1 \times)	82.0 67.6 (225.3 \times)

that terminating diffusion iterations early under appropriate confidence conditions is both feasible and safe. From these experiments, jointly enabling the three proposed modules yields the strongest overall results, demonstrating that each component in our framework is essential for achieving improved performance.

Prefill and generation length. We further investigate the effect of prefill and generation length. As shown in Table 4, increasing the prefill length from 3-shot to 8-shot reduces throughput for both Fast-dLLM and Streaming-dLLM. Nevertheless, compared to Fast-dLLM, the speedup of our method increases from $2.1\times$ to $2.9\times$, indicating that the proposed mechanism remains effective at alleviating inference time computational overhead even under longer prefill settings. On the other hand, as reported in Table 5, our method exhibits a pronounced advantage over Fast-dLLM in long-context generation. When the generation length reaches

Table 6. Impact of trailing positional information.

Model	Trailing Position	Accuracy (%)
Dream	✗	72.8
	✓	74.7
LLaDA	✗	77.5
	✓	78.7
LLaDA-1.5	✗	79.6
	✓	81.2

2048 tokens, it achieves a speedup of up to 225.3 \times relative to the vanilla model. Moreover, across all evaluated settings, our approach consistently outperforms Fast-dLLM in

terms of generation quality, demonstrating that our acceleration strategy not only improves efficiency but also enables dLLMs to better adapt to block-wise diffusion inference.

Trailing positional information. Discussion on the necessity of retaining trailing positional information is summarized in Table 6. It can be observed that omitting the trailing positional information leads to a noticeable drop in generation accuracy. Remarkably, this outcome is both intuitive and theoretically justified. When trailing positional information is not preserved, the model theoretical performance depends mainly on the block size and the number of retained suffix blocks, rather than the overall generation length. In practice, existing dLLMs typically rely on entire sequence positional information for global modeling, yet the experimental results suggest that this is not strictly required, as a small portion of the suffix combined with the final positional information can approximate the overall behavior. This finding provides new insight into enabling dLLMs to strike a more suitable balance between autoregressive and pure diffusion generation paradigms.

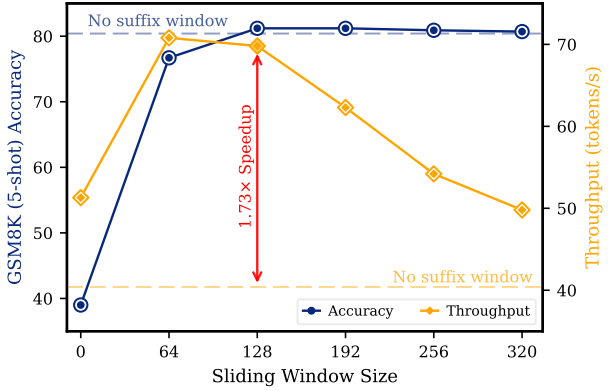


Figure 5. Ablation study on the sliding window size (no suffix windows, mean size = 512).

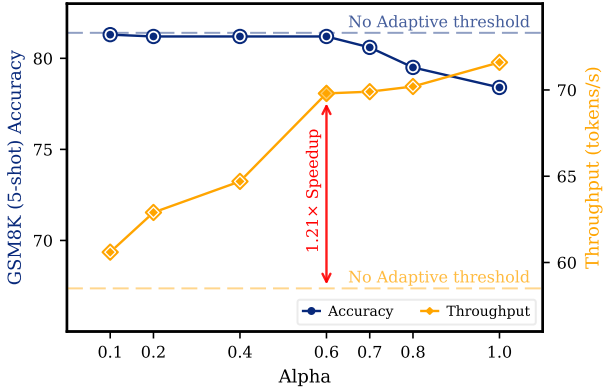


Figure 6. Effect of the parallel decoding parameter α (no adaptive threshold, mean $\alpha = 0$).

Hyperparameters. We further conduct ablation studies on key hyperparameters. We first examine the effect of the sliding window size w in Attenuation Guided Suffix Modeling. This parameter controls the fraction of the suffix region retained, balancing generation quality and inference efficiency. As shown in Figure 5, both accuracy and throughput improve as the window size increases. Once the window exceeds a certain threshold, accuracy saturates while throughput begins to decline. When $w = 128$, a favorable balance is achieved, where accuracy is slightly improved and a $1.73\times$ speedup is obtained relative to the full window size of 512. This result indicates that most suffix tokens contribute marginally to the generation of the current block, whose information can be sufficiently captured by a more compact near area, thereby confirming the presence of substantial computational redundancy in the suffix region.

We next study the effect of the parameter α , which controls parallel decoding. As reported in Figure 6, increasing α from 0.1 to 0.6 gradually improves throughput. However, further increasing α results in a degradation of overall performance, suggesting that overly aggressive threshold adjustments can adversely affect decoding stability and generation quality. This is likely due to premature parallel decoding of tokens that have not fully converged, causing confidence misalignment that accumulates across subsequent iterations.

5. Conclusion

We presented Streaming-dLLM, an efficient inference acceleration framework for dLLMs. The proposed method introduces Attenuation Guided Suffix Modeling to approximate the suffix region of the sequence by retaining only a small set of structurally informative regions. This design substantially reduces redundant computation in the spatial dimension during block-wise decoding. Building upon this, we further propose dynamic confidence-aware parallel decoding, which adaptively adjusts the degree of parallel decoding according to the dynamic evolution of token confidence across diffusion iterations. Combined with an early-exit mechanism, this strategy effectively avoids unnecessary denoising iterations for tokens that have already achieved sufficient confidence, thereby further reducing inference overhead in the temporal dimension. Overall, Streaming-dLLM effectively addresses the dual inefficiencies of existing dLLMs during inference in both the spatial and temporal dimensions. Extensive evaluations across multiple dLLMs benchmarks show that our method preserves Comparable performance while achieving up to $68.3\times$ inference speedup, demonstrating strong practicality and scalability.

Impact Statement

This paper presents work whose goal is to advance the field of machine learning by improving the efficiency of dLLMs. While more efficient generative models may broaden access and reduce energy consumption, they could also lower barriers to misuse, which is a general concern in this area of research. Aside from these widely recognized implications, we do not believe our work raises additional ethical or societal issues that must be specifically highlighted here.

References

Achiam, J., Adler, S., Agarwal, S., Ahmad, L., Akkaya, I., Aleman, F. L., Almeida, D., Altenschmidt, J., Altman, S., Anadkat, S., et al. Gpt-4 technical report. *arXiv preprint arXiv:2303.08774*, 2023.

Arriola, M., Gokaslan, A., Chiu, J. T., Yang, Z., Qi, Z., Han, J., Sahoo, S. S., and Kuleshov, V. Block diffusion: Interpolating between autoregressive and diffusion language models. *arXiv preprint arXiv:2503.09573*, 2025.

Austin, J., Johnson, D. D., Ho, J., Tarlow, D., and Van Den Berg, R. Structured denoising diffusion models in discrete state-spaces. *Advances in neural information processing systems*, 34:17981–17993, 2021a.

Austin, J., Odena, A., Nye, M., Bosma, M., Michalewski, H., Dohan, D., Jiang, E., Cai, C., Terry, M., Le, Q., et al. Program synthesis with large language models. *arXiv preprint arXiv:2108.07732*, 2021b.

Chen, M. Evaluating large language models trained on code. *arXiv preprint arXiv:2107.03374*, 2021.

Chen, T., Zhang, S., and Zhou, M. Dlm-one: Diffusion language models for one-step sequence generation. *arXiv preprint arXiv:2506.00290*, 2025a.

Chen, X., Huang, S., Guo, C., Wei, C., He, Y., Zhang, J., Li, H., Chen, Y., et al. Dpad: Efficient diffusion language models with suffix dropout. *arXiv preprint arXiv:2508.14148*, 2025b.

Cobbe, K., Kosaraju, V., Bavarian, M., Chen, M., Jun, H., Kaiser, L., Plappert, M., Tworek, J., Hilton, J., Nakano, R., et al. Training verifiers to solve math word problems. *arXiv preprint arXiv:2110.14168*, 2021.

Dubey, A., Jauhri, A., Pandey, A., Kadian, A., Al-Dahle, A., Letman, A., Mathur, A., Schelten, A., Yang, A., Fan, A., et al. The llama 3 herd of models. *arXiv preprint arXiv:2407.21783*, 2024.

Feng, G., Geng, Y., Guan, J., Wu, W., Wang, L., and He, D. Theoretical benefit and limitation of diffusion language model. *arXiv preprint arXiv:2502.09622*, 2025.

Gao, Z., Guo, J., Tan, X., Zhu, Y., Zhang, F., Bian, J., and Xu, L. Empowering diffusion models on the embedding space for text generation. In *Proceedings of the 2024 Conference of the North American Chapter of the Association for Computational Linguistics: Human Language Technologies (Volume 1: Long Papers)*, pp. 4664–4683, 2024.

Guo, D., Yang, D., Zhang, H., Song, J., Zhang, R., Xu, R., Zhu, Q., Ma, S., Wang, P., Bi, X., et al. Deepseek-r1: Incentivizing reasoning capability in llms via reinforcement learning. *arXiv preprint arXiv:2501.12948*, 2025.

Hendrycks, D., Burns, C., Basart, S., Zou, A., Mazeika, M., Song, D., and Steinhardt, J. Measuring massive multitask language understanding. *arXiv preprint arXiv:2009.03300*, 2020.

Li, T., Chen, M., Guo, B., and Shen, Z. A survey on diffusion language models. *arXiv preprint arXiv:2508.10875*, 2025.

Li, X., Thickstun, J., Gulrajani, I., Liang, P. S., and Hashimoto, T. B. Diffusion-lm improves controllable text generation. *Advances in neural information processing systems*, 35:4328–4343, 2022.

Lin, Z., Gong, Y., Shen, Y., Wu, T., Fan, Z., Lin, C., Duan, N., and Chen, W. Text generation with diffusion language models: A pre-training approach with continuous paragraph denoise. pp. 21051–21064, 2023.

Liu, A., He, M., Zeng, S., Zhang, S., Zhang, L., Wu, C., Jia, W., Liu, Y., Zhou, X., and Zhou, J. Wedlm: Reconciling diffusion language models with standard causal attention for fast inference. *arXiv preprint arXiv:2512.22737*, 2025a.

Liu, Z., Yang, Y., Zhang, Y., Chen, J., Zou, C., Wei, Q., Wang, S., and Zhang, L. dllm-cache: Accelerating diffusion large language models with adaptive caching. *arXiv preprint arXiv:2506.06295*, 2025b.

Ma, X., Yu, R., Fang, G., and Wang, X. dkv-cache: The cache for diffusion language models. *arXiv preprint arXiv:2505.15781*, 2025a.

Ma, Y., Du, L., Wei, L., Chen, K., Xu, Q., Wang, K., Feng, G., Lu, G., Liu, L., Qi, X., et al. dinfer: An efficient inference framework for diffusion language models. *arXiv preprint arXiv:2510.08666*, 2025b.

Mahabadi, R. K., Ivison, H., Tae, J., Henderson, J., Beltagy, I., Peters, M. E., and Cohan, A. Tess: Text-to-text self-conditioned simplex diffusion. In *Proceedings of the 18th Conference of the European Chapter of the Association for Computational Linguistics (Volume 1: Long Papers)*, pp. 2347–2361, 2024.

Nguyen-Tri, Q., Ranjan, M., and Shen, Z. Attention is all you need for kv cache in diffusion llms. *arXiv preprint arXiv:2510.14973*, 2025.

Nie, S., Zhu, F., You, Z., Zhang, X., Ou, J., Hu, J., Zhou, J., Lin, Y., Wen, J.-R., and Li, C. Large language diffusion models. *arXiv preprint arXiv:2502.09992*, 2025.

Sahoo, S., Arriola, M., Schiff, Y., Gokaslan, A., Marroquin, E., Chiu, J., Rush, A., and Kuleshov, V. Simple and effective masked diffusion language models. *Advances in Neural Information Processing Systems*, 37:130136–130184, 2024.

Song, Y., Liu, X., Li, R., Liu, Z., Huang, Z., Guo, Q., He, Z., and Qiu, X. Sparse-dllm: Accelerating diffusion llms with dynamic cache eviction. *arXiv preprint arXiv:2508.02558*, 2025a.

Song, Y., Zhang, Z., Luo, C., Gao, P., Xia, F., Luo, H., Li, Z., Yang, Y., Yu, H., Qu, X., et al. Seed diffusion: A large-scale diffusion language model with high-speed inference. *arXiv preprint arXiv:2508.02193*, 2025b.

Su, J., Ahmed, M., Lu, Y., Pan, S., Bo, W., and Liu, Y. Roformer: Enhanced transformer with rotary position embedding. *Neurocomputing*, 568:127063, 2024.

Tian, Y., Liang, Y., Sun, J., Zhang, S., Yang, G., Shu, Y., Fang, S., Guo, T., Han, K., Xu, C., et al. From next-token to next-block: A principled adaptation path for diffusion llms. *arXiv preprint arXiv:2512.06776*, 2025.

Wang, G., Schiff, Y., Sahoo, S. S., and Kuleshov, V. Remasking discrete diffusion models with inference-time scaling. *arXiv preprint arXiv:2503.00307*, 2025.

Wei, Q., Zhang, Y., Liu, Z., Liu, D., and Zhang, L. Accelerating diffusion large language models with slowfast: The three golden principles. *arXiv preprint arXiv:2506.10848*, 2025.

Wu, C., Zhang, H., Xue, S., Diao, S., Fu, Y., Liu, Z., Molchanov, P., Luo, P., Han, S., and Xie, E. Fast-dllm v2: Efficient block-diffusion llm. *arXiv preprint arXiv:2509.26328*, 2025a.

Wu, C., Zhang, H., Xue, S., Liu, Z., Diao, S., Zhu, L., Luo, P., Han, S., and Xie, E. Fast-dllm: Training-free acceleration of diffusion llm by enabling kv cache and parallel decoding. *arXiv preprint arXiv:2505.22618*, 2025b.

Wu, T., Fan, Z., Liu, X., Zheng, H.-T., Gong, Y., Jiao, J., Li, J., Guo, J., Duan, N., Chen, W., et al. Ar-diffusion: Auto-regressive diffusion model for text generation. *Advances in Neural Information Processing Systems*, 36:39957–39974, 2023.

Xu, G., Hao, J., Shen, L., Hu, H., Luo, Y., Lin, H., and Shen, J. Lgvit: Dynamic early exiting for accelerating vision transformer. In *Proceedings of the 31st ACM International Conference on Multimedia*, pp. 9103–9114, 2023.

Yang, A., Li, A., Yang, B., Zhang, B., Hui, B., Zheng, B., Yu, B., Gao, C., Huang, C., Lv, C., et al. Qwen3 technical report. *arXiv preprint arXiv:2505.09388*, 2025.

Ye, J., Xie, Z., Zheng, L., Gao, J., Wu, Z., Jiang, X., Li, Z., and Kong, L. Dream 7b: Diffusion large language models. *arXiv preprint arXiv:2508.15487*, 2025.

You, Z., Nie, S., Zhang, X., Hu, J., Zhou, J., Lu, Z., Wen, J.-R., and Li, C. Llada-v: Large language diffusion models with visual instruction tuning. *arXiv preprint arXiv:2505.16933*, 2025.

Yu, P., Xie, S., Ma, X., Jia, B., Pang, B., Gao, R., Zhu, Y., Zhu, S.-C., and Wu, Y. N. Latent diffusion energy-based model for interpretable text modeling. *arXiv preprint arXiv:2206.05895*, 2022.

Zhang, L., Fang, L., Duan, C., He, M., Pan, L., Xiao, P., Huang, S., Zhai, Y., Hu, X., Yu, P. S., et al. A survey on parallel text generation: From parallel decoding to diffusion language models. *arXiv preprint arXiv:2508.08712*, 2025.

Zhao, S., Gupta, D., Zheng, Q., and Grover, A. d1: Scaling reasoning in diffusion large language models via reinforcement learning. *arXiv preprint arXiv:2504.12216*, 2025.

Zhu, F., Wang, R., Nie, S., Zhang, X., Wu, C., Hu, J., Zhou, J., Chen, J., Lin, Y., Wen, J.-R., et al. Llada 1.5: Variance-reduced preference optimization for large language diffusion models. *arXiv preprint arXiv:2505.19223*, 2025a.

Zhu, F., You, Z., Xing, Y., Huang, Z., Liu, L., Zhuang, Y., Lu, G., Wang, K., Wang, X., Wei, L., et al. Llada-moe: A sparse moe diffusion language model. *arXiv preprint arXiv:2509.24389*, 2025b.

Zhu, Q., Yao, Y., Zhao, R., Xiang, Y., Saseendran, A., Jin, C., Teare, P., Liang, B., He, Y., and Gui, L. Latent refinement decoding: Enhancing diffusion-based language models by refining belief states. *arXiv preprint arXiv:2510.11052*, 2025c.

A. Details of Attention and Token Confidence Sampling Procedure

For Figure 2, we analyze the attention distribution at the final layer (Layer 31) of LLaDA-1.5, which captures interactions between the currently generated block and the full input sequence. Statistics are collected from 300 GSM8K samples with a generation length of 512. For each sample, the first 300 tokens of the prompt are treated as the prefix area; tokens in $[300:300+\text{block_size}]$ correspond to the currently generated block, while tokens in $[300+\text{block_size}:]$ form the suffix area. In the analysis, the solid line represents the mean attention score at each diffusion step, and the shaded area indicates the interquartile range (25%–75%). The results indicate that attention is largely concentrated on a few neighboring suffix blocks and the final token, whereas most intermediate positions in the suffix area receive negligible attention. This pattern suggests substantial redundancy in the suffix region during block-wise generation.

For Figure 3, we further examine the token confidence distribution during iterative block-wise generation of LLaDA-1.5 on GSM8K with a generation length of 256. Statistics are collected from the iterative decoding process of 100 samples, focusing on the first generated block. The results show that the mean token confidence steadily increases as iterations progress. While applying a high confidence threshold helps ensure generation quality, it can also be conservative, potentially delaying the acceptance of tokens that are already sufficiently confident.

Additional visualizations for more generation blocks are shown in the Figures 7 to 14. From these results, we observe that: (1) As iterations progress, blocks generated later tend to start with higher initial mean confidence, resulting in faster decoding. (2) In some decoding processes, the mean token confidence temporarily decreases. We attribute this behavior to a high confidence threshold, which forces many tokens back into the masked state, thereby affecting subsequent predictions. These observations further highlight the limitations of using a fixed confidence threshold in iterative block-wise generation.

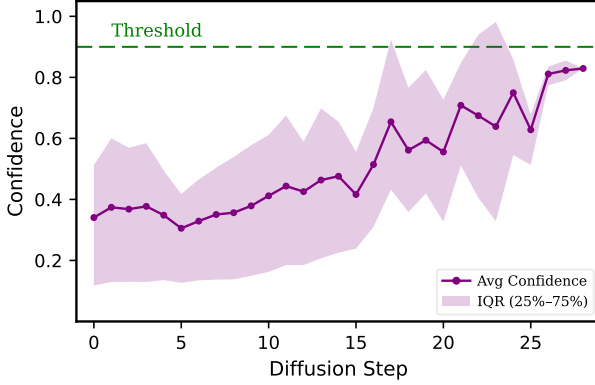


Figure 7. Token confidence distribution of block 0.

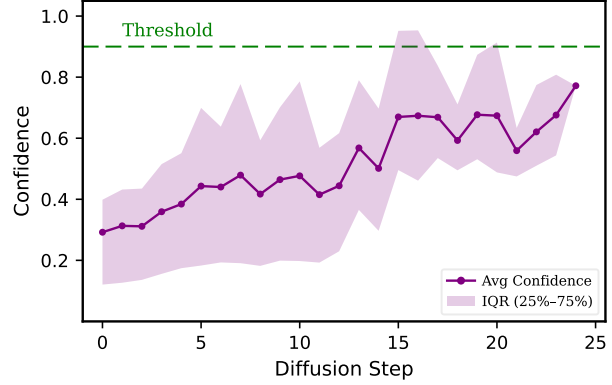


Figure 8. Token confidence distribution of block 1.

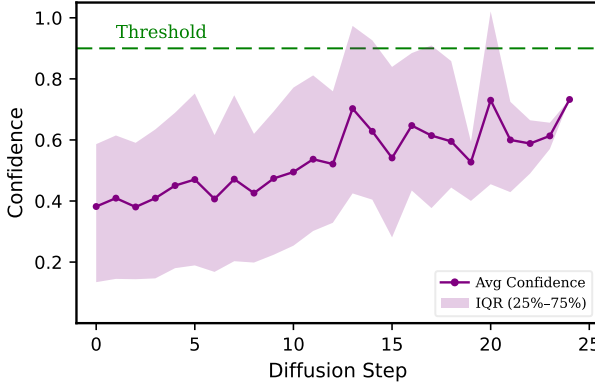


Figure 9. Token confidence distribution of block 2.

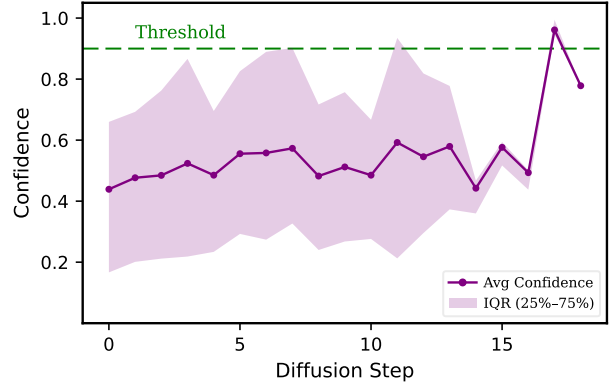


Figure 10. Token confidence distribution of block 3.

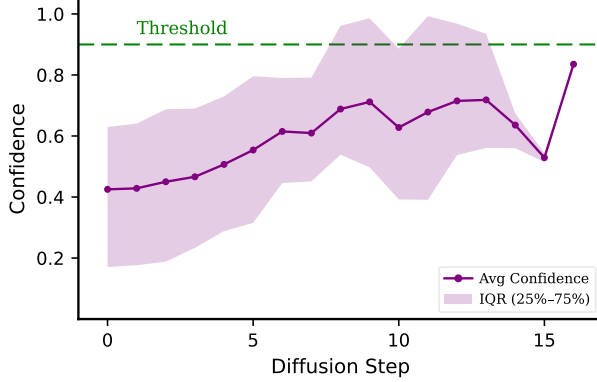


Figure 11. Token confidence distribution of block 4.

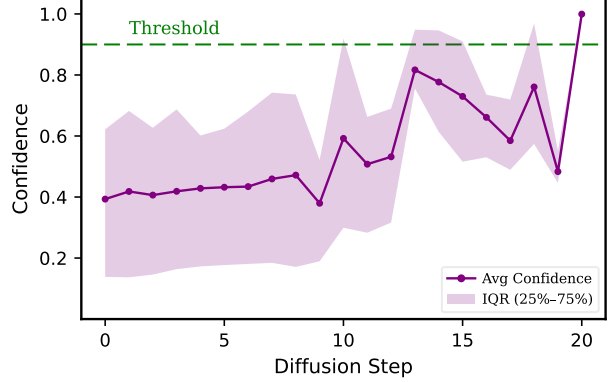


Figure 12. Token confidence distribution of block 5.

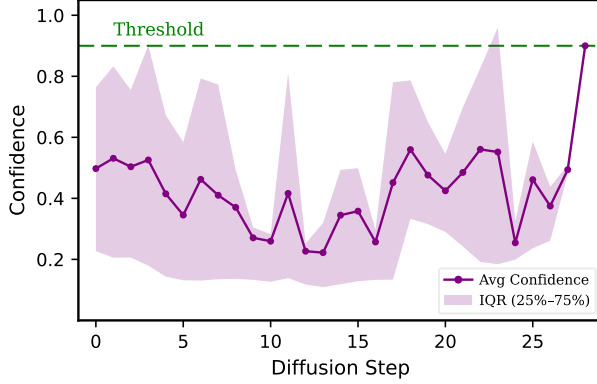


Figure 13. Token confidence distribution of block 6.

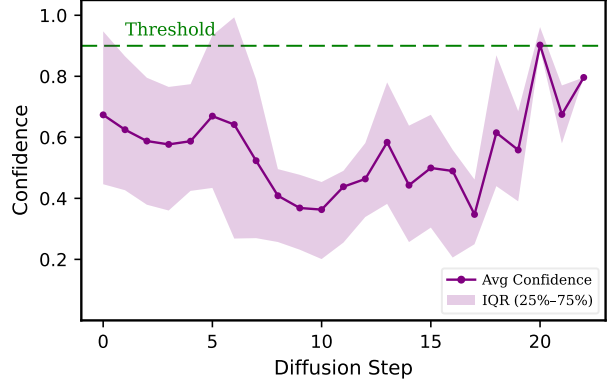


Figure 14. Token confidence distribution of block 7.

Table 7. Comparison of LLaDA-Instruct suite performance across four benchmarks at different generation lengths (256 and 512). Each cell reports accuracy (top) and decoding throughput with relative speedup over the LLaDA baseline (bottom; blue: tokens/s, orange: speedup). Results in bold indicate the highest score, while those underlined denote the second-best performance for each method. “*” marks results we reproduced using the official implementation, as they were not reported in the original papers.

Benchmark	Gen Length	LLaDA	dKV-Cache	Prefix-Cache	Fast-dLLM	Ours
HumanEval (0-shot)	256	41.5	39.6*	42.7	<u>43.3</u>	43.4
	512	18.4 (1×)	18.9 (1.0×)	30.6 (1.7×)	71.5 (3.9×)	93.3 (5.1×)
		43.9	45.1*	45.7	44.5	44.5
GSM8K (5-shot)	256	79.3	76.5*	79.5	78.5	78.5
	512	6.6 (1×)	11.6 (1.8×)	26.0 (3.9×)	50.9 (7.7×)	66.2 (10.0×)
		77.5	77.6*	77.0	77.2	78.7
MBPP (3-shot)	256	3.2 (1×)	5.5 (1.7×)	11.0 (3.4×)	32.1 (10.0×)	65.9 (20.6×)
	512	29.4	26.2*	29.6	28.2	42.0
		5.9 (1×)	10.0 (1.7×)	19.7 (3.3×)	44.3 (7.5×)	64.2 (10.9×)
MATH (4-shot)	256	14.8	14.6*	13.4	13.8	40.8
	512	4.2 (1×)	6.9 (1.6×)	12.6 (3.0×)	39.7 (9.4×)	66.7 (15.9×)
		33.5	33.3*	33.3	33.2	33.3
	256	8.7 (1×)	14.3 (1.6×)	29.0 (3.3×)	49.3 (5.7×)	71.0 (8.2×)
	512	37.2	36.3*	36.2	36.0	36.1
		6.2 (1×)	10.1 (1.7×)	18.6 (3.0×)	43.2 (7.0×)	63.2 (10.2×)

B. Additional Experiment Details.

B.1. More Experiments on LLaDA-Instruct

We report the accuracy and throughput results on LLaDA-Instruct in Table 7. Our method achieves $6.4\times$ – $20.6\times$ speedup across all tasks. In comparison, the second-best method, Fast-dLLM, achieves $4.4\times$ – $10.0\times$ speedup with slightly lower accuracy. Specifically, our method improves accuracy by 13.8%–27.0% on MBPP. We attribute this improvement to the proposed attenuation guided suffix modeling, which effectively suppresses interference from semantically weak, high-entropy masked tokens in the distant suffix region during block-wise generation.

B.2. Inference Latency Experiments for dLLMs

In addition, we compare Streaming-dLLM and several other baselines in terms of per sample inference latency. This metric better reflects user-perceived responsiveness in practical scenarios, highlighting the suitability of our method for real-time deployment (Xu et al., 2023). As shown in Table 8, Streaming-dLLM achieves a $4.8\times$ – $21.0\times$ speedup across all benchmarks compared with the vanilla backbone. Relative to the strongest acceleration baseline, it provides an additional $1.5\times$ – $4.5\times$ speedup on tasks with a generation length of 512, while maintaining comparable or slightly improved accuracy.

We observe even faster speed gains on LLaDA-1.5, as reported in Table 9. In particular, Streaming-dLLM attains a $52.7\times$ speedup on MBPP at generation length 512, markedly exceeding that of Fast-dLLM (Wu et al., 2025b). Consistent improvements are also evident on LLaDA-Instruct of Table 10, where our method achieves $5.3\times$ – $64.1\times$ speedup across all tasks. By comparison, the second-best method, Fast-dLLM, reaches only $3.9\times$ – $9.9\times$ speedup with slightly lower accuracy.

Overall, these results demonstrate that Streaming-dLLM consistently improves inference efficiency across different dLLM backbones and tasks without sacrificing generation quality. The substantial gains in both throughput and per sample latency highlight its practicality for real-world deployment, particularly in latency-sensitive and interactive applications.

Table 8. Comparison of Dream-Base suite performance across four benchmarks at different generation lengths (256 and 512). Each cell reports accuracy (top) and inference latency with relative speedup over the Dream baseline (bottom; blue: s, orange: speedup). Results in bold indicate the highest score, while those underlined denote the second-best performance for each method. ‘*’ marks results we reproduced using the official implementation, as they were not reported in the original papers.

Benchmark	Gen Length	Dream	dKV-Cache	Prefix-Cache	Fast-dLLM	Ours
HumanEval (0-shot)	256	49.4	48.2*	<u>53.7</u>	54.3	54.3
		11.9 (1.0×)	11.9 (1.0×)	<u>8.0 (1.5×)</u>	4.6 (2.6×)	<u>2.5 (4.8×)</u>
	512	54.3	49.4*	54.9	54.3	<u>54.6</u>
GSM8K-CoT (5-shot)	256	74.8	73.6*	<u>74.0</u>	73.5	<u>74.0</u>
		<u>18.6 (1.0×)</u>	<u>15.0 (1.2×)</u>	<u>8.1 (2.3×)</u>	5.3 (3.5×)	<u>2.1 (8.9×)</u>
	512	<u>74.2</u>	71.6*	<u>74.2</u>	74.1	74.7
MBPP (3-shot)	256	56.6	54.0*	53.2	56.4	<u>56.4</u>
		<u>23.3 (1.0×)</u>	<u>17.4 (1.3×)</u>	<u>7.7 (3.0×)</u>	<u>3.8 (6.1×)</u>	<u>3.3 (7.1×)</u>
	512	<u>55.6</u>	53.0*	53.8	55.2	55.8
MATH (4-shot)	256	38.4	36.8*	36.8	<u>37.6</u>	<u>37.6</u>
		<u>24.5 (1.0×)</u>	<u>17.5 (1.4×)</u>	<u>7.9 (3.1×)</u>	4.2 (5.8×)	<u>3.2 (7.7×)</u>
	512	39.8	38.5*	38.0	39.3	<u>39.4</u>
		<u>59.3 (1.0×)</u>	<u>44.1 (1.3×)</u>	<u>20.9 (2.8×)</u>	9.4 (6.3×)	<u>5.2 (11.4×)</u>

Table 9. Comparison of LLaDA-1.5 suite performance across four benchmarks at different generation lengths (256 and 512). Each cell reports accuracy (top) and inference latency with relative speedup over the LLaDA-1.5 baseline (bottom; blue: s, orange: speedup). Results in bold indicate the highest score, while those underlined denote the second-best performance for each method. ‘*’ marks results we reproduced using the official implementation, as they were not reported in the original papers.

Benchmark	Gen Length	LLaDA-1.5	dKV-Cache	Prefix-Cache	Fast-dLLM	Ours
HumanEval (0-shot)	256	43.9*	<u>40.2*</u>	38.4*	37.2*	39.0
		<u>12.7 (1.0x)</u>	12.7 (1.0x)	<u>7.72 (1.6x)</u>	4.2 (3.0x)	<u>2.3 (5.5x)</u>
		40.5*	<u>40.2*</u>	37.8*	39.8*	<u>40.2</u>
	512	<u>38.2 (1.0x)</u>	<u>32.4 (1.2x)</u>	<u>21.2 (1.8x)</u>	<u>7.6 (5.0x)</u>	<u>2.9 (13.2x)</u>
		80.5*	<u>80.7*</u>	80.6*	<u>80.7</u>	80.8
		<u>34.5 (1.0x)</u>	<u>20.1 (1.7x)</u>	<u>8.9 (3.9x)</u>	<u>4.4 (7.8x)</u>	<u>2.0 (17.3x)</u>
GSM8K (5-shot)	256	81.0*	81.3*	81.0*	80.4	<u>81.2</u>
		<u>81.8 (1.0x)</u>	<u>48.1 (1.7x)</u>	<u>24.3 (3.4x)</u>	<u>7.8 (10.5x)</u>	<u>2.2 (37.2x)</u>
	512	<u>38.0*</u>	38.2*	37.8*	37.6*	37.8
		<u>28.7 (1.0x)</u>	<u>17.7 (1.6x)</u>	<u>8.5 (3.4x)</u>	<u>2.3 (12.5x)</u>	<u>1.2 (23.9x)</u>
MBPP (3-shot)	256	<u>38.2*</u>	38.1*	38.0*	38.1*	38.4
		<u>68.5 (1.0x)</u>	<u>43.0 (1.6x)</u>	<u>23.1 (3.0x)</u>	<u>4.1 (16.7x)</u>	<u>1.3 (52.7x)</u>
	512	<u>32.7*</u>	31.8*	32.5*	32.6	33.7
		<u>27.9 (1.0x)</u>	<u>17.6 (1.6x)</u>	<u>8.5 (3.3x)</u>	<u>4.7 (5.9x)</u>	<u>2.7 (10.3x)</u>
MATH (4-shot)	256	37.1*	<u>35.1*</u>	35.0*	<u>35.1</u>	<u>35.1</u>
		<u>66.3 (1.0x)</u>	<u>42.1 (1.6x)</u>	<u>22.9 (2.9x)</u>	<u>8.4 (7.9x)</u>	<u>4.6 (14.4x)</u>

Table 10. Comparison of LLaDA-Instruct suite performance across four benchmarks at different generation lengths (256 and 512). Each cell reports accuracy (top) and inference latency with relative speedup over the LLaDA baseline (bottom; blue: s, orange: speedup). Results in bold indicate the highest score, while those underlined denote the second-best performance for each method. ‘*’ marks results we reproduced using the official implementation, as they were not reported in the original papers.

Benchmark	Gen Length	LLaDA	dKV-Cache	Prefix-Cache	Fast-dLLM	Ours
HumanEval (0-shot)	256	41.5	<u>39.6*</u>	42.7	<u>43.3</u>	43.4
		<u>13.3 (1.0x)</u>	<u>12.9 (1.0x)</u>	<u>7.9 (1.7x)</u>	<u>3.4 (3.9x)</u>	<u>2.5 (5.3x)</u>
		43.9	<u>45.1*</u>	45.7	44.5	44.5
	512	<u>39.4 (1.0x)</u>	<u>32.9 (1.2x)</u>	<u>21.4 (1.8x)</u>	<u>9.0 (4.4x)</u>	<u>5.2 (7.6x)</u>
		<u>79.3</u>	76.5*	79.5	78.5	78.5
		<u>35.5 (1.0x)</u>	<u>20.2 (1.8x)</u>	<u>9.0 (3.9x)</u>	<u>4.6 (7.7x)</u>	<u>2.2 (16.1x)</u>
GSM8K (5-shot)	256	77.5	<u>77.6*</u>	77.0	77.2	78.7
		<u>84.1 (1.0x)</u>	<u>49.0 (1.7x)</u>	<u>24.7 (3.4x)</u>	<u>8.5 (9.9x)</u>	<u>2.3 (36.6x)</u>
	512	29.4	<u>26.2*</u>	<u>29.6</u>	28.2	42.0
		<u>29.4 (1.0x)</u>	<u>17.6 (1.7x)</u>	<u>8.6 (3.4x)</u>	<u>3.8 (7.7x)</u>	<u>0.9 (32.7x)</u>
MBPP (3-shot)	256	14.8	14.6*	13.4	13.8	40.8
		<u>70.5 (1.0x)</u>	<u>43.3 (1.6x)</u>	<u>23.6 (3.0x)</u>	<u>7.6 (9.3x)</u>	<u>1.1 (64.1x)</u>
	512	33.5	<u>33.3*</u>	<u>33.3</u>	33.2	<u>33.3</u>
		<u>28.6 (1.0x)</u>	<u>17.4 (1.6x)</u>	<u>8.6 (3.3x)</u>	<u>5.1 (5.6x)</u>	<u>3.5 (8.2x)</u>
MATH (4-shot)	256	37.2	<u>36.3*</u>	36.2	36.0	36.1
		<u>68.8 (1.0x)</u>	<u>42.7 (1.6x)</u>	<u>23.3 (3.0x)</u>	<u>10.0 (6.9x)</u>	<u>6.8 (10.1x)</u>

B.3. Optimization and Schedule.

We provide detailed configurations for evaluation on Humaneval, GSM8K, MBPP, and MATH, as summarized in Table 11. For each benchmark and backbone (Dream, LLaDA, and LLaDA-1.5), we report the generation length, sliding window size, initial confidence threshold τ_0 , decay factor α , and block size used in our experiments. For all models, the block size is set to 32 across datasets, while other hyperparameters vary by benchmark and generation length. These settings are consistently applied for runs reported in the main paper.

Table 11. Configurations for different dataset.

Model	Benchmark	Gen Length	sliding window size	τ_0	α	block_size
Dream	Humaneval (0-shot)	256	192	0.9	0.7	32
		512	128	0.9	0.4	32
	GSM8K-CoT (5-shot)	256	32	0.9	0.3	32
		512	32	0.9	0.3	32
	MBPP (3-shot)	256	192	0.9	0.3	32
		512	192	0.9	0.6	32
	MATH (4-shot)	256	32	0.9	0.1	32
		512	32	0.9	0.3	32
LLaDA	Humaneval (0-shot)	256	192	0.9	0.3	32
		512	256	0.9	0.4	32
	GSM8K (5-shot)	256	96	0.9	0.3	32
		512	96	0.9	0.3	32
	MBPP (3-shot)	256	32	0.9	0.3	32
		512	32	0.9	0.3	32
	MATH (4-shot)	256	128	0.9	0.3	32
		512	256	0.9	0.2	32
LLaDA-1.5	Humaneval (0-shot)	256	96	0.9	0.3	32
		512	96	0.9	0.4	32
	GSM8K (5-shot)	256	96	0.9	0.4	32
		512	128	0.9	0.6	32
	MBPP (3-shot)	256	96	0.9	0.3	32
		512	96	0.9	0.3	32
	MATH (4-shot)	256	96	0.9	0.4	32
		512	192	0.9	0.3	32

B.4. Additional Analysis for Generation Length.

Table 12. Impact of generation length on Accuracy and Speedup for LLaDA on GSM8K (5-Shot).

Model	512	1024	2048
LLaDA	77.5	77.6	76.8
	3.2 (1 \times)	1.1 (1 \times)	0.4 (1 \times)
Fast-dLLM	77.2	75.3	76.4
	32.1 (10.0 \times)	15.0 (13.6 \times)	6.5 (16.3 \times)
Ours	78.7	78.3	78.7
	65.9 (20.6 \times)	64.7 (58.8 \times)	67.1 (167.8 \times)

Table 12 reports the accuracy and speedup of LLaDA on GSM8K (5-shot) under different generation lengths (512, 1024, and 2048). For each model, the top row shows the accuracy, while the bottom row reports the throughput (tokens per second) in blue and the corresponding speedup relative to the vanilla backbone in orange. The results indicate that our method

consistently maintains high accuracy across all generation lengths while achieving substantially larger speedup compared with both LLaDA and Fast-dLLM, especially as the generation length increases.